Am J Transl Res 2021;13(8):8921-8937
www.ajtr.org /ISSN:1943-8141/AJTR0133467

Original Article

Influence of fixation on CA4+ contrast enhanced microCT of articular cartilage and subsequent feasibility for histological evaluation

Xueqin Gao[1,2], Amit N Patwa[3,4], Zhenhan Deng[2], Hajime Utsunomiya[1], Mark W Grinstaff[3], Joseph J Ruzbarsky[1], Brian D Snyder[5], Sudheer Ravuri[1], Marc J Philippon[1], Johnny Huard[1,2]

[1]Steadman Philippon Research Institute, Vail, CO, USA; [2]Department of Orthopaedic Surgery, McGovern Medical School, University of Texas Health Science Center at Houston, Houston, TX, USA; [3]Department of Biomedical Engineering, Boston University, Boston, MA, USA; [4]Current Institution, School of Science, Navrachana University, Vadodara, Gujarat, India; [5]Center for Advanced Orthopaedic Studies, Beth Israel Deaconess Medical Center, Harvard Medical School, Boston, MA, USA

Received March 23, 2021; Accepted June 9, 2021; Epub August 15, 2021; Published August 30, 2021

Abstract: CA4+ is a novel cationic iodinated contrast agent utilized for contrast-enhanced microCT (CECT). In this study, we compared CA4+ CECT for cartilage quantification of unfixed and neutral buffered formalin (NBF)-fixed rabbit distal femur cartilage after 8-, 24- and 30-hours of contrast agent diffusion. The stability of CA4+ binding to cartilage after PBS soak and decalcification was also investigated by CECT. We further assessed the feasibility of cartilage histology and immunohistochemistry after CA4+ CECT. Contrast-enhanced CA4+ labeled unfixed and NBF-fixed cartilage tissues facilitate articular cartilage quantification and accurate morphological assessment. The NBF fixed tissues demonstrate higher cartilage intensity and imaging characteristics distinct from subchondral bone than unfixed tissues while maintaining stable binding even after decalcification with 10% EDTA. The unfixed tissues labeled with CA4+, after CECT imaging and decalcification, are amenable to H&E, Alcian blue, and Safranin O staining, as well as Col2 immunohistochemistry. In contrast, only H&E and Alcian blue staining can be accomplished with CA4+ labeled NBF fixed cartilage, and CA4+ labeling interferes with downstream immunohistochemistry and Safranin O staining, likely due to its positive charge. In conclusion, CA4+ CECT of NBF fixed tissues provides high quality microCT cartilage images and allows for convenient quantification along with feasible downstream H&E and Alcian blue staining after decalcification. CA4+ CECT of unfixed tissues enables researchers to obtain both quantitative microCT as well as cartilage histology and immunohistochemistry data from one set of animals in a cost-, time-, and labor-efficient manner.

Keywords: CA4+, contrast enhanced microCT, cartilage imaging, histology

Introduction

Osteoarthritis (OA) treatment alternatives to arthroplasty remain a clinical challenge. In order to meet this challenge with new therapies (i.e., biologics), it is important to elucidate mechanism(s) of OA development using a variety of experimental OA models such as destabilized medial meniscus (DMM) [1-3], anterior cruciate ligament transaction (ACT) [4-6], meniscus ligament injury (MLI) [7-10] and chemical induced OA [11]. Conventionally, the evaluation of the injured cartilage, its healing, and repair relies upon two-dimensional (2D) histology using staining and immunohistochemistry techniques for extracellular matrix components such as collagen and glycosaminoglycans (GAGs) as well as cells including chondrocytes [12-16]. Although histology and immunohistochemistry reveal the 2D cartilage structure, microstructural components, and changes at the molecular level, 3D reconstruction of the entire articular cartilage offers more quantitative data as well as improved information on the spatial relationships amongst areas of interest.

Micro-computed tomography (MicroCT) is a commonly used imaging modality for bony tis-

sues based on x-ray attenuation [17]. It is an excellent tool for 3D imaging and quantification of calcified tissues; however, it has not yet been optimized for imaging of cartilage and other soft tissues. To expand its application, contrast agents are needed to enhance the detection of soft tissues in a technique referred to as contrast-enhanced CT (CECT). Several contrast agents have been described for CECT of cartilage based on different principles. For example, phosphotungstic acid (PTA) binds the collagenous matrix of cartilage, generating increased radiodensity than bone along with good correlations with histology grading (R^2 = 0.8708, P<0.0001 for cartilage thickness, and R^2 = 0.7606, P<0.0001 for cartilage volume) [18, 19]. A 3D histopathological grading scale of osteochondral tissues, based on PTA contrast-enhanced microCT (PTA-CECT), could detect cartilage lesions [19]. Furthermore, PTA-CECT, when combined with finite element modeling enables assessment of cartilage mechanics [18]. The PTA-collagen binding in PTA-labeled tissues is reversible, allowing for washing and downstream cartilage staining [19]. But, unfortunately, given PTA's toxicity, it is not used for *in vivo* cartilage imaging. In addition, it is a very acidic molecule that can harm the tissues and cause stiffening of tissues. Another contrast agent is Ioxaglate sodium (Hexabrix 320) which has a negative (anionic) charge and as a result its x-ray attenuation inversely correlates with GAG content in cartilage [20, 21]. However, it was discontinued in 2015 due to its adverse effects when applied *in vivo*. Therefore, developing new agents for contrast enhanced microCT is a priority.

More recently, cationic CECT reagents were developed such as the cationic iodinated contrast agent, 5,5'-(malonylbis(azanediyl)) bis (N1,N3-bis(2-aminoethyl)-2,4,6-triiodoisophthalamide (CA4+). The CA4+ contrast agent has 4 positive charges and 6 iodine atoms and was first designed and synthesized for CECT of cartilage [22, 23]. The CA4+ contrast-imaged microCT cartilage demonstrates greater x-ray attenuation and a larger dynamic range when compared to tissues treated with anionic contrast agents. CA4+ CECT successfully imaged *ex vivo* bovine and human menisci [24, 25], equine cartilage defects [26, 27], human cartilage [23, 28, 29], mouse tibia plateau cartilage and endochondral bone formation [28, 30] as well as *in vivo* rabbit cartilage [31] and tissue engineered chondrogenic pellets [32]. The resulting contrast-enhanced attenuation positively correlates with the content and location of GAGs within the tissue. Furthermore, CA4+ contrast attenuation also correlates with cartilage stiffness [33] and other biomechanical properties [34]. Additionally, non-calcified cartilage thickness measured using CA4+ CECT strongly correlates with cartilage thickness measured by histology (R^2 = 0.72. P<0.001) [35]. It can also detect cartilage degeneration (measured by volume and thickness) in mice of different ages [35]. Using CA4+ for CECT provides greater sensitivity for evaluation of GAG content and shows similar results to those obtained using the anionic contrast agent Hexabrix for the quantification of cartilage volume and thickness [35].

CECT using CA4+ has been reported for *ex vivo* imaging of human trapeziometacarpal cartilage to assess gross structure and morphology as well as mechanical properties [36]. Recently, dual contrast imaging of human cartilage using clinical grade full body CT and CA4+/gadoteridol showed promise for simultaneous measurement of cartilage, water (Gadoteridol), and GAG (CA4+) content [29, 37]. In an equine impact-induced cartilage injury model, *in vivo* CA4+ CECT x-ray attenuation negatively correlated with cumulative Osteoarthritis Research Society International (OARSI) histology score (Safranin O staining based, R = -0.61, P< 0.0001) [38].

Given the abundant application and utility of CA4+ CECT, the aims of this study were to investigate whether CA4+ can be used to image fixed rabbit cartilage tissues, to determine the stability of the CA4+ staining protocol, and to assess the feasibility of downstream histology and immunohistochemistry after CA4+ CECT.

Materials and methods

CA4+ synthesis and contrast labeling

5,5'-(malonylbis (azanediyl)) bis (N1,N3-bis(2-aminoethyl)-2,4,6-triiodoisophthalamide (CA-4+) was synthesized as previously described [23] in the Grinstaff's laboratory at Boston University and shipped to the Huard laboratory at the University of Texas Health Science Center in Houston. It has 4 positive charges and 6

iodine atoms and was first designed and synthesized by Grinstaff's laboratory for CECT of cartilage [20, 21]. The use of animals for this study was approved by the Institutional Animal Care and Use Committee of University of Texas Health Science Center at Houston (AWC-17-0022). Rabbit distal femurs were dissected from the uninjured side of 6-7 month-old New Zealand white rabbits (Charles River) that were used for previous investigations to minimize animal sacrifice. These rabbits previously underwent generation of a patellar groove osteochondral defect with microfracture and either losartan oral treatment [39] or bevacizumab intra-articular injection [40]. In total, 40 distal femur tissues were used for this study. The distal femur tissues were divided into 2 groups: the unfixed group and the 10% neutral buffered formalin (Sigma-Aldrich, HT501128-4L) fixed cartilage group (NBF fixed). N = 5 was used for each group and each diffusion time and No CA4+ groups. For the unfixed group, all the rabbit distal femurs were dissected and stored at -80°C prior to CA4+ contrast labeling and imaging. For the NBF fixed group, distal femurs were fixed in NBF for 10 days or 4 months at room temperature until CA4+ labeling because no differences were found for NBF fixation time. Both groups of tissues were washed with PBS, immersed in 10 mL CA4+ (24 mg/ml, pH = 7.4, 400 mOsm/Kg) as reported before [23, 38] and then agitated on a horizontal shaker at 60 rpm and room temperature for 8, 24, and 30 hours. Three samples were labeled and scanned for each diffusion time of the two groups due to the size of the microCT scan holder. This was also because CA4+ labeling may require immediate scanning of samples after labeling to ensure signaling is maintained. The tissues were then subjected to microCT imaging at 8, 24, and 30 hours after labeling as detailed below.

MicroCT scanning

Immediately after CA4+ contrast staining for all 30 samples of both groups, the distal femurs with intact joint cartilage were rinsed with deionized water for 2 minutes, wrapped with parafilm and scanned with a Viva CT 40 using 70 kVp, 114 μA, x-ray energy and 38 μm resolution (voxel size). The scanning parameters were integration time/averaging (200 ms/1), 1024×1024 size, calibration: BH, 1200 mgHA/cm^3. In total, 550-650 slices were scanned in about 30 minutes for each sample to cover the entire distal femur joint. After scanning, the samples were placed in sterile PBS (magnesium and calcium free, pH 7.4) for 5 days at 4°C and then scanned via microCT using the same parameters to determine the stability of CA4+ binding. After the second round of microCT scanning following PBS soaking, both groups of distal femur tissues were decalcified in 10% ethylenediaminetetraacetic disodium (EDTA) plus 1% sodium hydroxide (pH 7.2) for 4 months. Samples in the unfixed femur group were kept unfixed during the entirety of the decalcification process. The same cohort of distal femurs were then scanned a third time via microCT using the same protocol (control file) after decalcification as stated above.

MicroCT 3D analysis

SCANCO Medical MicroCT software (Brüttisellen, Switzerland) was utilized by manually contouring 50 slices of femur patellar groove cartilage at the axial level of the condyle, allowing both the patellar groove and condyle cartilage to be visualized (axial view). A sigma = 1, gauss support = 0.8, threshold = 280 was chosen for 3D quantification. This threshold is 60 higher than the threshold used for rabbit trabecular bone (threshold = 220). Because there is no software for cartilage volume quantification, most studies transferred DICOM data to another software system such as Analyze™ [29] or Seg3D software to analyze [41]. We adopted the concept of bone volume and density quantification for bone in microCT software for cartilage volume and density quantification. The total contoured cartilage volume (view of interest) based on CA4+ CECT (total volume), total volume density (cartilage density), bone volume (cartilage volume, BV), and bone volume density (cartilage density) were automatically generated by the software for 3D quantification. The total volume represents view of interest. The bone volume given by the microCT quantification data here is actually cartilage volume which is defined by contouring high intensity tissues above subchondral trabecular bone, and was segmentalized by applying thresholds. The BV density is in essence cartilage density which represents GAGs contents that are bound by CA4+ through electrostatic charges. In addition, 2D microCT

images were converted to DICOM images and downloaded for visualization. Furthermore, DICOM images from microCT were converted into TIFF files using photoshop CC (Adobe, San Jose, CA, USA). TIFF files of 100 slices of microCT 2D images were then used to create videos using Image J to show the CA4+ contrast-labeled cartilage on the patellar groove and condyle in a continuous view. Representative videos were generated using 24 h labeling of NBF fixed and unfixed tissues both at the time immediately following staining and after decalcification.

Cartilage thickness measurement

For both unfixed and NBF fixed microCT images captured immediately following CA4+ contrast labeling, cartilage thickness measurements were performed at three different locations using microCT 3D distance measuring tools: central patellar groove (thickest cartilage), patellar groove periphery (midpoints between groove and ridge), and condyle cartilage. The thickness measured was the same as the 3D slices range (50 slices) and measured every 5 slices. Each sample's cartilage thickness was an average of 10 measurements and was shown as mm.

Histology

After undergoing microCT scans, the tissues were then processed using gradient ethanol, cleared with xylene, and embedded in paraffin. 5 μm thickness paraffin sections were cut using a microtome. H&E staining was then performed after section mounting using Sigma Harris Hematoxylin and Eosin Y reagents (Sigma. St. Louis, MO, USA). Alcian blue staining was performed using the IHC world protocol (http://www.ihcworld.com/_protocols/special_stains/alcian_blue.htm) with the reagents Alcian Blue 8GX and nuclear fast red (Sigma). Safranin O staining was performed using the IHC world protocol with modification by staining for 30 minutes (http://www.ihcworld.com/_protocols/special_stains/safranin_o.htm).

Immunohistochemistry

Paraffin slides of all groups were deparaffinized and rehydrated. Antigen retrieval was performed using 2% hyaluronidase (H3506, Sigma-Aldrich/Millipore) in PBS (pH = 7.4) at room temperature for 30 minutes. Slides were then washed with PBS and incubated with 5% donkey serum in PBS at room temperature for 1 hour. The sections were then incubated with mouse anti-collagen II (Col2) (MA1-37493, Invitrogen/Fisher [Hampton, NH, USA]) at 1:200 dilution at 4°C overnight. On the second day, the slides were washed with PBS. The slides were then immersed in 0.5% hydrogen peroxide in PBS for 30 minutes to inactivate endogenous hydrogen peroxidase. After an additional wash with PBS, slides were incubated with biotinylated horse anti-mouse secondary antibody (BA2000, Vector Laboratories, Burlingame, CA, USA) for 2 hours at room temperature. The slides were subsequently incubated using the Elite ABC kit (PK-6100, Vector Laboratories) after PBS washes. DAB color reaction was performed using the DAB Kit (SK-4100, Vector Laboratories) for 6 minutes. Slides were rinsed with tap water thoroughly and nuclei counterstaining was performed using Hematoxylin QS (Vector Laboratories, H-3404-100) for 20 seconds. Subsequently, slides were rinsed in running tap water for 10 minutes before dehydration using gradient ethanol and xylene and then cover slipped with a xylene based Cytoseal mount medium (Fisher Scientific).

Statistical analysis

Power analysis was performed based on previous microCT analysis to determine sample size. All values are mean ± SD. Statistical analysis was performed using Microsoft Excel (Redmond, WA, USA). The Student t-test was used for comparisons amongst groups at each time point; $P<0.05$ was considered statistically significant.

Results

CA4+ CECT of NBF fixed cartilage shows improved cartilage image quality compared to unfixed cartilage

CA4+ effectively stained the patellar groove and condyle cartilage that covered the subchondral trabecular bone and demonstrated a higher radiodensity than subchondral bone in both unfixed and NBF fixed groups at 8, 24, and 30 hours after labeling. The femoral cartilage in the NBF fixed samples was more easily distinguished from subchondral bone than in the unfixed tissues (**Figure 1A**). For the tissues not treated with CA4+, the cartilage was indis-

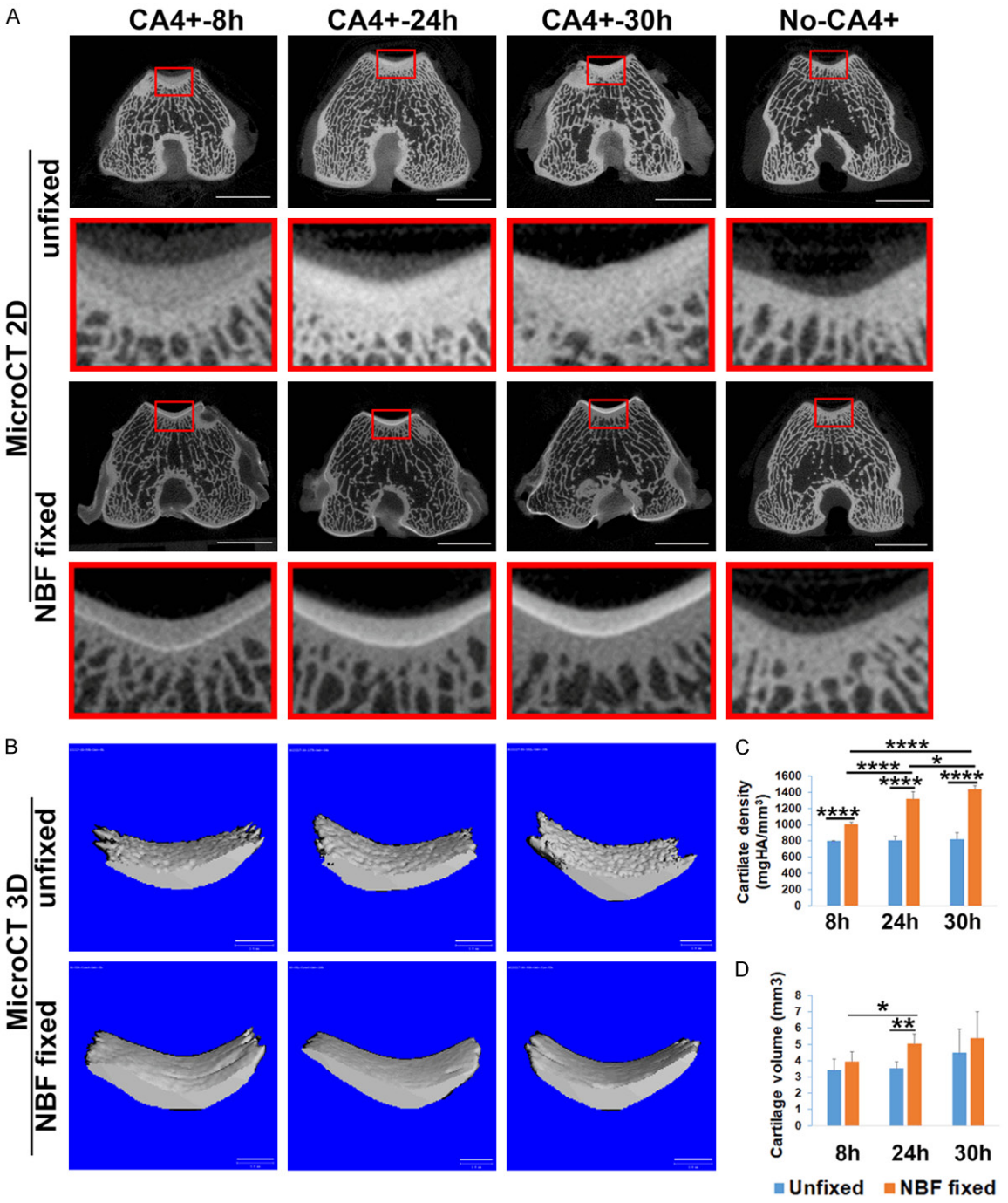

Figure 1. Comparison of CA4+ CECT results of unfixed and NBF fixed cartilage at different incubation times. A. 2D microCT images of CA4+ CECT for unfixed and NBF fixed cartilage at different time points. Red boxes represent enlargements from original images of the patellar groove cartilage. For the unfixed tissues, articular cartilage intensity (attenuation) is enhanced and visible but not easily distinguishable from subchondral bone, while in the no-CA4+ (control) tissue, cartilage is not visible. For NBF fixed tissues, cartilage showed higher intensity than subchondral bone at all time points (8, 24, 30 hours). In the NBF fixed no-CA4+ samples, cartilage is not visible compared to surrounding area. Scale bar = 5 mm. B. Micro3D images of 50 slices patellar groove cartilage for NBF fixed and unfixed tissues. Cartilage surface in the unfixed groups appears rough (lower density) while that of NBF fixed cartilage appears smooth. Scale bar in 3D images is 1 mm. C. Comparison of cartilage density (intensity). NBF fixed tissues showed significantly higher density than those of unfixed cartilage density. In addition, 24 and 30 hours labeling also showed significantly higher density than the 8-hour incubation time for NBF fixed cartilage. There were no significant differences between 24 and 30 hours incubations compared to the 8 hours incubation for unfixed tissues. $^{*}P<0.05$, $^{****}P<0.0001$. D. Cartilage volume showed no statistical differences between unfixed cartilage and NBF fixed cartilage at 8 and 30 hours. However, at 24 hours, the NBF group showed higher cartilage volume. $^{*}P<0.05$; $^{**}P<0.01$.

tinguishable in both unfixed and NBF fixed groups (**Figure 1A**). MicroCT 3D images showed that the cartilage surface of the patellar groove of NBF fixed tissues was smoother and had higher density at 8, 24 and 30 hours post-contrast staining relative to unfixed cartilage by applying the same threshold (**Figure 1B**). The continuous views of 24 hour labeling of NBF fixed and unfixed cartilage are shown in Supplementary Videos 1 and 2, respectively. The NBF fixed cartilage tissue density (attenuation) was significantly higher than that of the unfixed CA4+ contrast labeled tissue group at all three diffusion times (**Figure 1C**, $P = 1.9\times10^{-6}$, 4.72×10^{-5}, and 2.14×10^{-7} for the 8, 24 and 30 hour diffusion times, respectively, for the NBF fixed group versus unfixed group). For the NBF fixed group, the 24 and 30 hour labeling times also showed significant higher cartilage density than 8 hours. A time-dependent labeling of cartilage density was observed for NBF fixed tissues ($R^2 = 0.9999$, $P = 0.062$). The correlation coefficient of time and density for unfixed femoral tissues was less significant ($R^2 = 0.8381$, $P = 0.2636$) (**Figure 1C**). Cartilage volume was not statistically different for both groups for 8 and 30 hour labeling groups. But at 24 hours, NBF fixed cartilage showed significant higher cartilage volume. This discrepancy may be caused by the labeling density difference between the two groups (**Figure 1D**, $P = 0.0064$). However, the total volume which showed the cartilage tissue size based on CA4+ CECT showed no difference between the two groups at 8, 24 and 30 hours labeling ($P = 0.50$, 0.10, 0.35 respectively for 8, 24 and 30 hours labeling time point, data not shown).

CA4+ CECT of unfixed and NBF fixed tissues both yields accurate cartilage thickness measurement

When measuring cartilage thickness for both unfixed and NBF fixed femoral cartilage after CA4+ labeling on representative 2D images at different axial levels, the NBF-fixed CA4+ labeled cartilage structures were more distinguishable with easier identification of the cartilage boundary when compared to the CA4+ labeled, unfixed cartilage tissues (**Figure 2A**). Three regions of cartilage were measured: the center of the patellar groove cartilage (the thickest area between two red arrows), the center between patellar groove and ridge (between two blue arrows), and the condyle cartilage (between two yellow arrows) (**Figure 2A**). No statistical differences were found for the cartilage thickness in the three locations of distal femur between CA4+ labeled unfixed and NBF fixed cartilage (**Figure 2B-D**). These results indicate that it is feasible to measure cartilage thickness accurately using CA4+ CECT for both unfixed and NBF fixed cartilage.

CA4+ binds cartilage in NBF fixed tissues in a more stable manner than in unfixed tissues after PBS wash

After soaking the CA4+ CECT labeled tissues in PBS for 5 days, the cartilage layer intensity of unfixed cartilage with CA4+ contrast staining for 8 and 24 hours decreased significantly when compared to the signal immediately following CA4+ labeling. However, some signal was still visible for the samples stained with CA4+ for 30 hours. In contrast, the NBF fixed femoral cartilage did not lose signal intensity at any time point when compared to fresh CA4+ labeled cartilage and exhibited consistently distinguishable articular cartilage from subchondral bone (**Figure 3A**). By contouring the patellar groove cartilage and applying the same threshold, the cartilage signal in 3D images in both the 8 and 24 hours labeled unfixed tissues was almost invisible, whereas there was still visible signal at the 30 hours labeling duration (**Figure 3B**). In contrast, the attenuation of the patellar groove cartilage was almost identical to fresh labeled tissues in the NBF fixed tissue group at all time points (**Figure 3B**). Quantification of the 3D microCT of cartilage density revealed a significantly higher cartilage density in NBF fixed tissues than unfixed CA4+ labeled tissues at all labeling time points (**Figure 3C**, $P = 9.4\times10^{-10}$, 9.7×10^{-8}, 6.8×10^{-5} respectively for the 8, 24 and 30 hours time points). The cartilage volumes at different labeling times were also significantly higher in the NBF fixed group than those of the unfixed group (**Figure 3D**, $P = 6.9\times10^{-7}$, 4.2×10^{-5}, 1.6×10^{-4} for 8, 24, 30 hours diffusion times, respectively). These results indicated that CA4+ binding to the NBF fixed cartilage is more stable, while the CA4+ binding in the unfixed cartilage can be washed out in PBS (reversible).

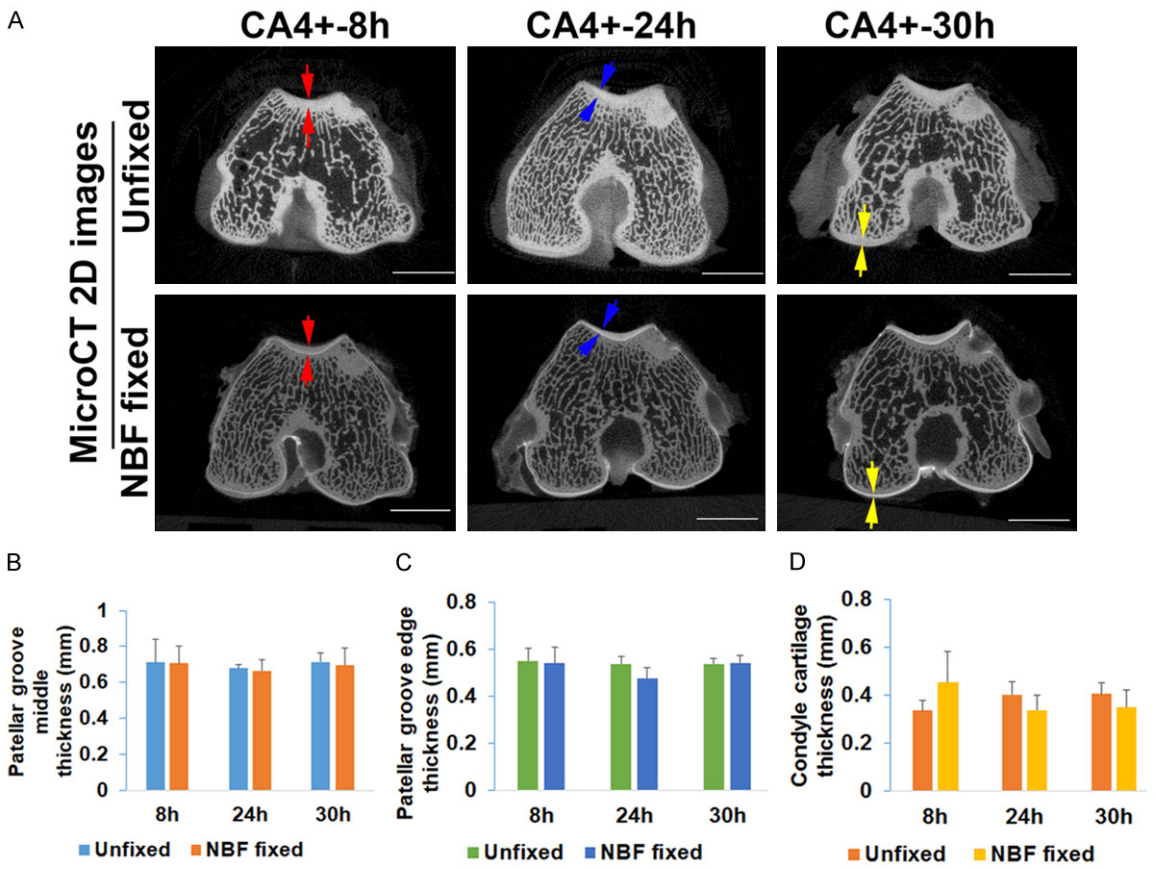

Figure 2. Measurement of cartilage thickness of CA4+ CECT microCT 2D images. A. Comparison of cartilage thickness of CA4+ contrasted unfixed tissues and NBF fixed tissues. Representative red arrows point to the patellar groove cartilages at the deepest concavity where articular cartilage is the thickest. Representative blue pairs of arrows indicate the cartilage thickness at the midpoint between the center of the groove and the lateral extent. Pairs of yellow arrows indicate the region of the condyle articular cartilage. Articular cartilage in NBF fixed cartilage is more easily defined than unfixed tissues. Scale bars = 5 mm. B. Comparison of the cartilage thickness at deepest patellar groove level showed no statistical difference between unfixed and NBF fixed cartilage. C. Cartilage thickness at the point between deepest and shallowest patellar groove cartilage showed no statistical difference between unfixed and NBF fixed tissues. D. Measurement of cartilage thickness at the condyle cartilage showed no statistical difference between unfixed and NBF fixed groups. The slightly variations were likely caused by the animal size variation rather than the accuracy of contouring for cartilage for both unfixed and NBF fixed groups of cartilage.

CA4+ labeled cartilage signal is maintained in NBF fixed tissues compared to loss of signal in unfixed femur tissue after decalcification

The distal femur tissues were microCT scanned after 4 months of decalcification. The results showed that the signal in the unfixed cartilage had completely disappeared for all diffusion time points (**Figure 4A**, upper panel). Subchondral bone signal was also not visible due to decalcification. A continuous view of the microCT images is shown in Supplementary Video 3. In contrast, the NBF fixed samples showed visualization of cartilage structure while subchondral trabecular bone was not visible due to decalcification. The signal is easily distinguishable and enables easy identification and contouring. Some residual subchondral bone that was not fully decalcified can still be visualized as seen in **Figure 4A** (lower panel). The distinct cartilage contrast images are also clearly demonstrated in a continuous view seen in Supplementary Video 4. The control samples without CA4+ contrast (No-CA4+) in both groups demonstrated no signal after decalcification (**Figure 4A**). MicroCT 3D images demonstrated that, after decalcification, the patellar groove cartilage appeared as distinct as both fresh-labeled and PBS soaked for 5 days at all three labeling time points (**Figure**

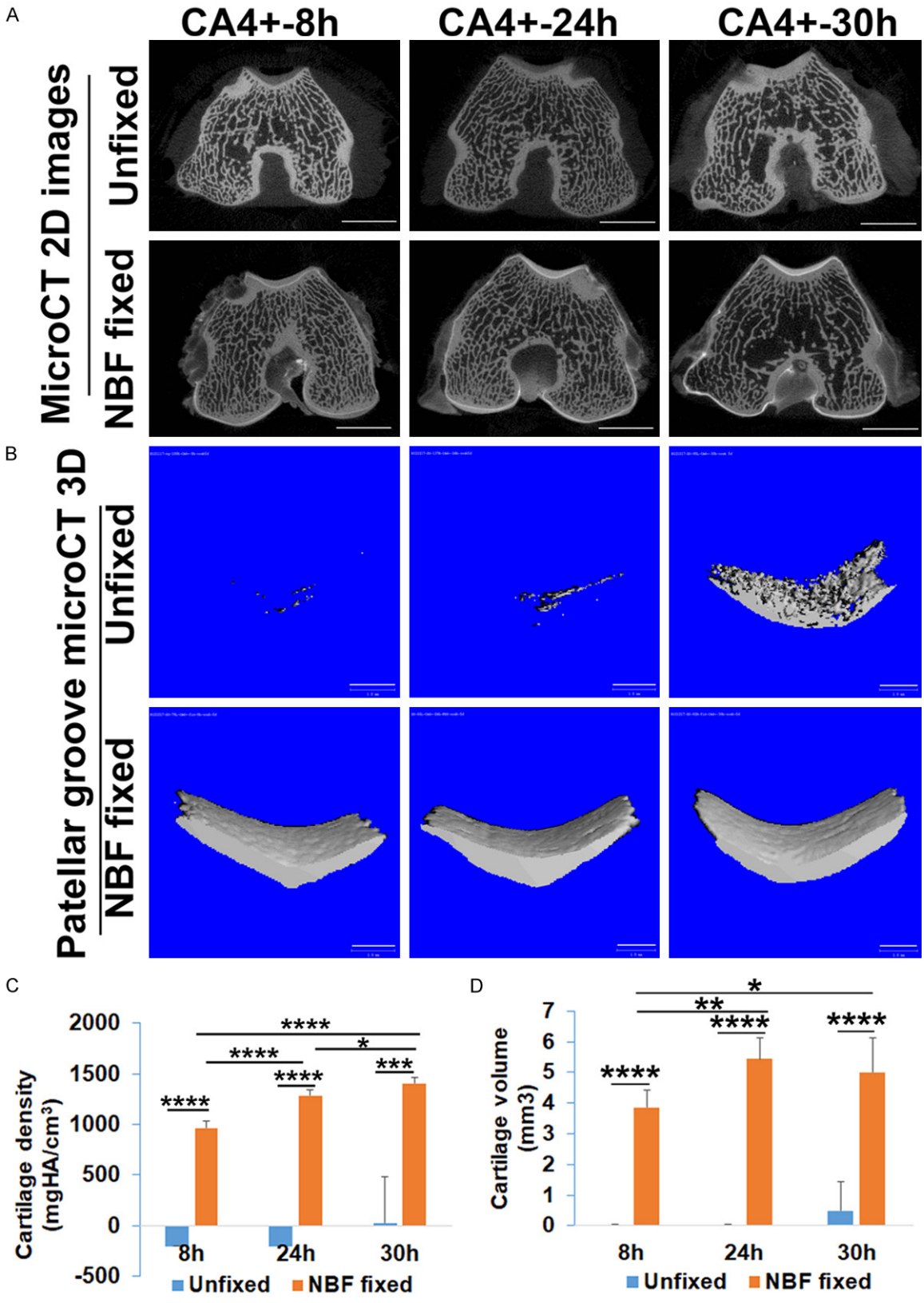

Figure 3. The stability of CA4+ CECT after PBS soaking. A. 2D microCT images showed significant signal decrease in the cartilage of unfixed tissues at 8 and 24 hours of incubation time at both the groove and condyle locations. The cartilage in the 30-hour group also showed intensity reduction. In contrast, the cartilage of the NBF fixed groups

showed no decrease in signal with a more distinguishable interface between articular cartilage and subchondral bone. Scale bars = 5 mm. B. MicroCT 3D images of 50 slices of patellar groove cartilage. The signal of cartilage in unfixed tissues significantly diminished with faint visible cartilage when using the same threshold as for fresh labeled cartilage. In contrast, NBF fixed cartilage demonstrates intense cartilage image morphology. Scale bars = 1 mm. C. Cartilage densities are significantly higher in NBF fixed tissues than unfixed tissues. $^{*}P<0.05$, $^{***}P<0.001$. D. Cartilage volumes are significantly higher in NBF fixed cartilage than those in unfixed cartilage at all tested time points. $^{*}P<0.05$, $^{**}P<0.01$, $^{****}P<0.0001$.

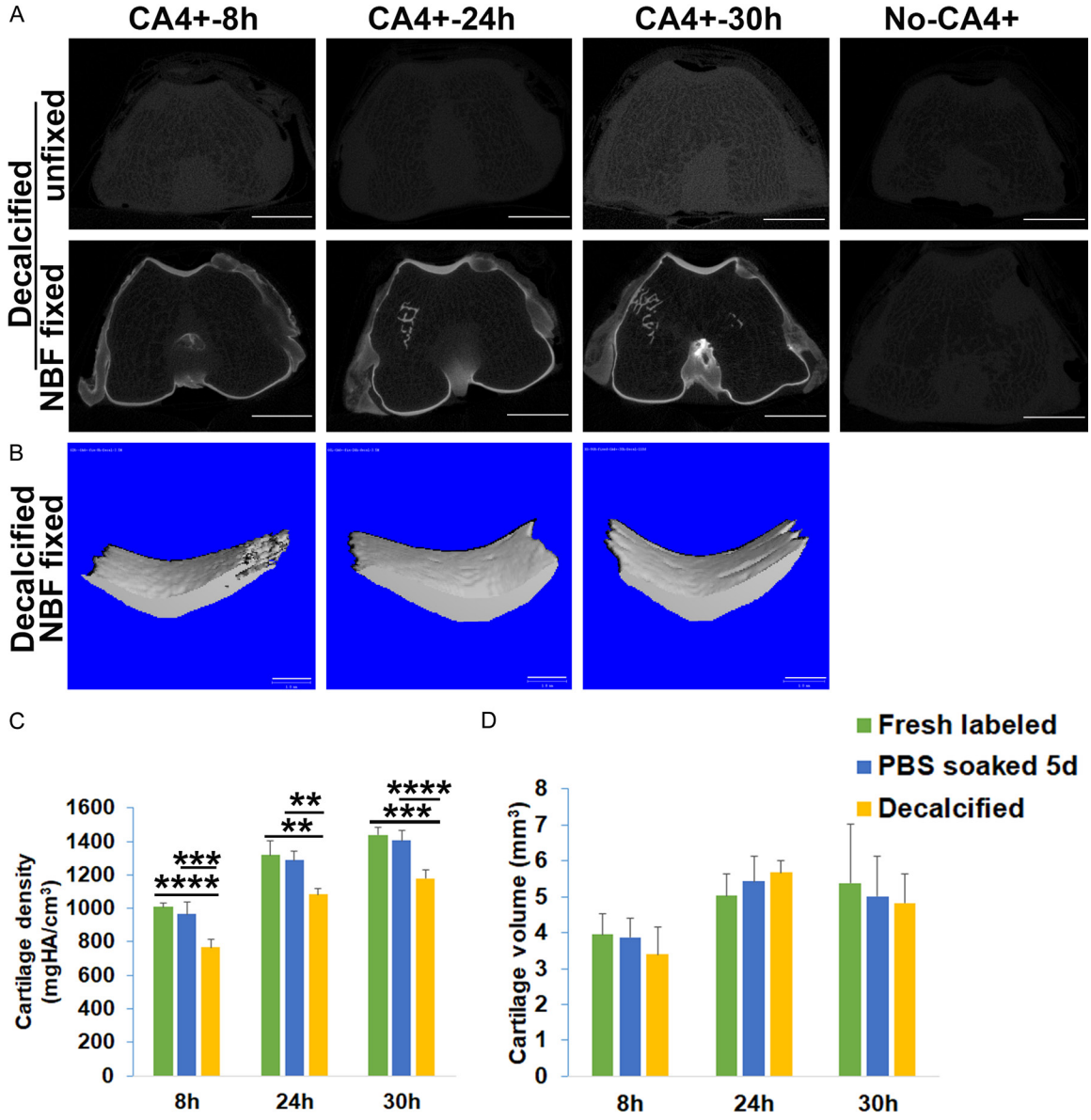

Figure 4. CA4+ labeled cartilage imaging after decalcification. A. 2D images of cartilage at the patellar groove level. The unfixed tissues have lost cartilage and bone signal after decalcification. Bone is not visible in the no-CA4+ labeled tissues. In contrast, the cartilage signal at the patellar groove and condyle of NBF fixed tissues showed visible cartilage structure. No signal is visualized in the subchondral bone except for residual trabecular bone in the 24- and 30-hour CA4+ labeled tissues. Scale bars = 5 mm. B. Micro3D image demonstrates clearly defined patellar groove cartilage and condyle cartilage in the NBF fixed cartilage after decalcification. Scale bars = 1 mm. C. Comparison of cartilage density for fresh CA4+ labeled, PBS soaked, and decalcified NBF fixed tissues. Specimens soaked in PBS for 5 days did not cause signal loss compared to fresh-labeled cartilage. Decalcification caused approximately a 20% decrease in density compared to fresh labeled and PBS soaked tissues. $^{**}P<0.01$, $^{***}P<0.001$, $^{****}P<0.0001$. D. Quantification of cartilage volume showed no statistical differences after decalcification compared to fresh labeled, PBS soaked for 5 days.

4B). Quantification of cartilage density of fresh labeled, PBS soaked, and decalcified NBF fixed cartilage demonstrated that PBS soaking did not cause intensity loss, while decalcification did result in approximately 20% decrease in cartilage density compared to both fresh labeled tissues and PBS soaked tissues in the NBF fixed tissue group at all time points (**Figure 4C**, $P = 4.52\times10^{-7}$, 0.0023, 3.56×10^{-6} respectively compared to fresh labeled for 8, 24 and 30 hours; $P = 1.86\times10^{-4}$, 8.0×10^{-4}, 5.24×10^{-5} compared to PBS soaked tissues for 8, 24, and 30 hours, respectively). However, the cartilage volume quantification did not change after decalcification (**Figure 4D**). These results indicate that, for NBF fixed CA4+ contrasted cartilage, it is feasible to quantify cartilage volume and thickness accurately even after decalcification. In contrast, cartilage could not be identified after decalcification for unfixed CA4+ labeled cartilage and therefore was not measured. These results indicate that the NBF fixed CA4+ labeled tissues are stable, with CA4+ signal remaining in the tissue after decalcification. As subchondral bone signal was removed after decalcification, only CA4-labeled cartilage signal can be visualized, thus enhancing ability to quantify cartilage (volume, thickness).

Histology

H&E staining demonstrated that the unfixed CA4+ labeled cartilage showed similar morphology as the No-CA4+ labeled cartilage tissues in the patellar groove cartilage. However, the nuclear stains in the subchondral bone were not intense in all CA4+ labeled unfixed tissues. The NBF fixed tissue group exhibited enhanced red cytoplasm color in the cartilage layer that could be distinguished from subchondral bone at all time points. A clear boundary delineation between cartilage and subchondral bone at the tidemark cartilage area was identified. This observation indicated that the binding of CA4+ to cartilage was specific (**Figure 5A**). Alcian blue staining showed blue cartilage matrix in the unfixed CA4+ labeled tissues at all time points, which was nearly the same as the No-CA4+ labeled cartilage tissues. NBF fixed tissues also showed blue matrix. Qualitatively and quantitatively, the subchondral bone residual blue stained cartilage matrix was equivalent to that of the No-CA4+ labeled NBF fixed group. However, there is a pink layer between cartilage and subchondral bone which showed residual blue cartilage matrix (**Figure 5B**, pointed by black arrows). Safranin O staining for unfixed CA4+ labeled tissues revealed orange-red cartilage staining, which was comparable to that of No-CA4+ labeled unfixed cartilage. However, for CA4+ contrasted NBF fixed tissue, the cartilage was not stained orange-red by Safranin O staining while No-CA4+ labeled fixed cartilage stained orange-red in the cartilage layer (**Figure 5C**). This result indicates that CA4+ specifically binds to GAG, similarly to Safranin O, which also possesses a positive charge, and likely inhibited Safranin O staining.

Immunohistochemical staining of Col2 showed the presence of Col2 positive matrix in unfixed CA4+ contrasted femur cartilage layers (brown) which were similar to no-CA4+ labeled unfixed cartilage. However, cartilage of CA4+ labeled NBF fixed tissues was negative for Col2 at 8, 24 and 30 hours labeling times, while the No-CA4+ labeled fixed cartilage showed robust brown Col2 positive staining in the cartilage layer (**Figure 5D**). These results correlated with the stable presence of CA4+ even after decalcification in NBF fixed cartilage.

Discussion

In this study, CECT with CA4+ staining to image *ex vivo* unfixed and NBF fixed rabbit distal femur articular cartilage was investigated as well as its effect on downstream histology commonly used for comprehensive cartilage evaluation. For unfixed tissues labeled with CA4+, cartilage could be visualized, but could not be easily distinguished from subchondral bone especially at longer diffusion times. Furthermore, it was feasible to perform both histology and immunohistochemistry for unfixed CA4+ labeled tissues after decalcification. In contrast, for the NBF fixed tissues, CECT cartilage images were distinct and exhibited a time-dependent increase in x-ray attenuation or intensity with CA4+ incubation time. H&E and Alcian blue staining were successful after decalcification for NBF fixed cartilage, however, Safranin O staining and immunohistochemistry were interfered with due to the presence of CA4+ even after decalcification in the cartilage layer, likely due to its positive charges.

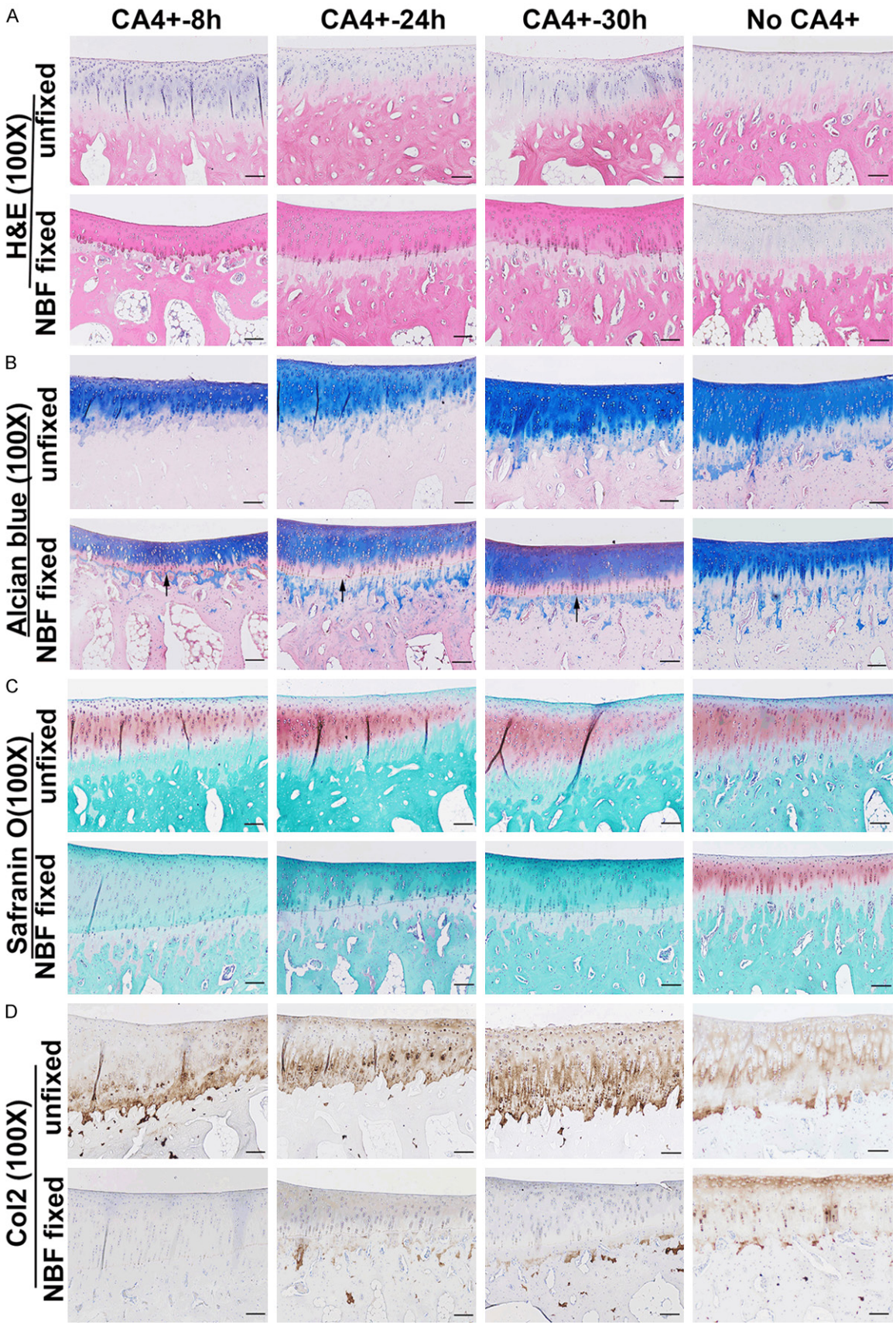
A
CA4+-8h
CA4+-24h
CA4+-30h
No CA4+
H&E (100X)
unfixed
NBF fixed
B
Alcian blue (100X)
unfixed
NBF fixed
C
Safranin O(100X)
unfixed
NBF fixed
D
Col2 (100X)
unfixed
NBF fixed

Figure 5. Histology of CA4+ contrasted unfixed and NBF fixed cartilage. A. H&E staining. CA4+ labeled unfixed cartilage stained similarly to no-CA4+ labeled control cartilage. The cartilage layer showed faint blue color in the cytoplasm. NBF fixed cartilage showed pink staining at the cartilage layer above the tidemark which differed from the no-CA4+ labeled NBF fixed cartilage which stained light blue. Cells and structures are clearly visible. B. Alcian staining showed that CA4+ contrasted unfixed cartilage is stained blue and the same as no-CA4+ labeled cartilage. CA4+ contrasted NBF fixed cartilage also showed a blue cartilage layer, however, there is a region of pink staining (black arrows) near the tidemark compared to no-CA4+ labeled NBF fixed cartilage. C. Safranin O staining. CA4+ contrasted unfixed cartilage showed a similar orange-red pattern to no-CA4+ labeled unfixed cartilage. However, CA4+ contrasted NBF fixed cartilage showed no orange-red staining in the cartilage layer while the no-CA4+ labeled NBF fixed cartilage stained positive for safranin O staining. D. Immunohistochemistry of Col2. CA4+ contrasted unfixed cartilage showed Col2 positivity at the cartilage layer which is similar to the no-CA4+ labeled unfixed cartilage. In contrast, CA4+ contrasted NBF fixed cartilage showed negative staining at the entire cartilage layer while the subchondral bone had positive staining in the residual cartilage matrix as brown color matrix. The no-CA4+ labeled NBF fixed cartilage showed Col2 positive in the cartilage layer. The slight color difference between CA4+ labeled and no CA4+ labeled either unfixed or NBF fixed cartilage was because staining was performed at different times. Scale bars = 100 μm for all the images.

CA4+ CECT imaging is a relatively new cartilage imaging technology. Its advantages include attenuation values which positively correlate with GAG concentration and equilibrium moduli as well as a greater dynamic range of attenuation values compared to images obtained using anionic contrast agents. Previous studies employing the CA4+ contrast agent primarily used unfixed cartilage tissues [34, 36, 37, 42], and only one study used fixed tissues from mice [35], but did not directly compare between unfixed and fixed tissues. The goal of the current study was to establish a protocol to optimize the use of one set of animals to gain multi-sets of data pertinent to cartilage analysis using CA4+ CECT. Most of the previous studies using CA4+ CECT did not focus on the entire view of the cartilage area nor did they provide volume and density quantification [27]. Therefore, in this study we evaluated the use of the microCT quantification system to perform 3D quantification of cartilage density, volume, and thickness using CA4+ CECT.

In this study, the results demonstrate that CA4+ contrast labeled unfixed tissues not only allow us to quantify cartilage volume and thickness using microCT built-in software, but the same tissues also retain their suitability for routine cartilage histology and immunohistochemistry evaluation. Consistent with this study's results, a previous study showed that tissues can be soaked overnight in a preservative solution to remove CA4+, followed by fixation with NBF, and then decalcification with formic acid to allow for downstream H&E and Safranin O staining. However, these investigators did not perform immunohistochemistry [38]. A previous study using human cadaver hand cartilage joint tissues for CA4+ CECT showed that Safranin O staining was also feasible for unfixed tissues [43]. Previously, it also has been shown that cartilage tissues undergoing CECT with ioxaglate sodium before fixation, and then fixed with formalin after CECT allowed further downstream histology evaluation using H&E and Safranin O staining [44, 45]. However, we noticed the nuclear stain in the subchondral bone was decreased in all staining which may be caused by tissue degradation as we did not fix the tissue for the entire process for CA4+ labeled unfixed cartilage. This can be avoided by fixing the tissues after the PBS soak following imaging as previously reported [38]. This study also demonstrated that the CA4+ labeling of unfixed tissues was reversible and can be removed by soaking in PBS. Hence, CA4+ labeling is not permanent and suitable for live animal imaging. Indeed, CA4+ has been used *in vivo* for equine cartilage imaging 4 hours after intraarticular injection [38]. Therefore, CA4+ is a promising contrast agent for CECT of unfixed *ex vivo* cartilage (and *in vivo* live cartilage imaging) and for the diagnosis of cartilage injury, while permitting generation of multi-sets of data using just one set of animal tissues.

The findings in this study are impactful as the protocol enables a researcher to obtain both quantitative MicroCT and histology data for cartilage using a single set of animals or specimens, which is both time and resource optimizing. In most experimental designs, many animals are potentially euthanized at the same time, but since labeling often needs to be performed in a batch-by-batch basis, the process might introduce potential inconsistences in the contrast labeling amongst specimens, especially when leaving samples at room temperature or 4°C. Therefore, after tissue harvest, it is

recommended that all samples are frozen at -80°C for future contrast labeling and scanning to be performed on a batch basis to maintain consistency.

Importantly, this study also demonstrated that CA4+ CECT for NBF fixed cartilage is more distinguishable from subchondral bone than CA4+ labeled unfixed tissues. CA4+ labeling is stable and the samples did not lose signal after a PBS soak of 5 days with very distinctive imaging of the articular cartilage after decalcification. The reason why the CA4+ labeled cartilage showed more distinguishable morphology and high density is unknown. This may be due to the increased attenuation values, i.e., signal obtained. However, it is not because the subchondral bone hydroxyapatite decreased, as it is common practice to scan bone specimen in NBF. A previous study investigated the influence of formalin fixation on equilibrium partitioning of anionic contrast agent with microCT tomorgraphy (EPIC-CT) of the anionic contrast agent ioxaglate, and demonstrated that formalin fixation decreased x-ray attenuation by 14.3% [46]. Furthermore, the attenuation (density) of EPIC-CT inversely correlates with GAG contents and high GAG contents will demonstrate lower attenuation because more anionic ioxaglate molecules are expelled. The observed decrease in x-ray attenuation in formalin fixed tissue occurred because more anionic agent was expelled. In this study, we used the cationic CA4+ contrast agent and found that formalin fixation enhanced attenuation which means increased binding of CA4+ on GAG despite its similar contents. Since the previous study showed that this difference was not due to GAG contents or the physical properties of cartilage [46], we believe that the influence of formalin fixation on CECT microCT images may be caused by cross links formed by formalin fixation which act to stabilize the negative charges in GAG of cartilage. Because the two contrast-enhanced agents have opposite electric charges, our results are in fact consistent with this previous study [46]. CA4+ has further advantages because formalin fixation increased the attenuation and distinction from subchondral bone.

A second advantage of CECT using NBF fixed cartilage is that it allows for subsequent H&E staining and Alcian blue staining despite the color being slightly different from No-CA4+ labeled NBF fixed tissues. The cartilage structure and cell components are easily identified. However, Safranin O, also a cationic molecule which primarily binds to GAGs, no longer stained the articular cartilage layer, but still stained the subchondral cartilage residual GAG as the CA4+ diffusion stopped at the cartilage tidemark. This result reinforces that CA4+ binding to cartilage is specific to GAGs, which is similar to the binding of Safranin O to GAGs. In addition to the inability to subsequently perform Safranin O staining, it was also not feasible to perform subsequent Col2 immunohistochemistry. This is possibly due to the strong CA4+ cartilage signals still present as shown in microCT scanning even after decalcification which may prevent the antigen-antibody binding. Hence, the disadvantage of using NBF fixed cartilage is that it is difficult to use one set of animals to perform both microCT quantification and a complete set of histology. While the advantage of using NBF fixed cartilage is that one can obtain more distinguishable CECT cartilage images and the tissues can be stored for many days in formalin at room temperature.

Why CA4+ remains in the NBF fixed cartilage after decalcification with EDTA is not known. Formalin's active molecule is formaldehyde, which forms cross-links between proteins via binding to lysine, tyrosine, asparagine, tryptophan, histidine, arginine, cysteine, and glutamine in all the proteins present in a specimen. These cross-links may prevent the dissociation of CA4+ from its binding protein GAG or the CA4+ bound to reactive sites remaining in the tissue due to the fixation process.

It has been shown that for formalin-fixed cartilage treated with 30% Hexabrix™ 320 for CECT, Safranin O [47] and Toluidine blue [48] staining can be performed after decalcification. In contrast to CA4+, the mechanism as to why it remains feasible to perform Safranin O after a Hexabrix stain likely relates to its anionic nature. The anionic Hexabrix does not avidly bind to the negatively charged GAGs and thus does not block Safranin O staining (in fact, Hexabrix remaining in the tissue may artificially increase the Safranin O signal). In the current study, the absence of the Safranin O staining signal after decalcification of CA4+ contrast labeled NBF fixed cartilage was likely due to the

negative charge of the GAG bound to CA4+ which prevented Safranin O binding. Another study investigated the effects of formalin fixation on CECT x-ray attenuation. The tissues were labeled with Hexabrix, microCT scanned, fixed with formalin, and again scanned with microCT. These investigators found that formalin fixation reduced x-ray attenuation by 11%, but the specimens retained propensity for later Safranin O and H&E staining which was likely due to Hexabrix's anionic nature [49]. Furthermore, it was previously demonstrated that using the PTA-contrast agent for cartilage imaging after formalin fixation allows downstream Safranin O staining and H&E staining after a 70% ethanol wash [18, 19]. These results may be explained by the hypothesis that PTA binds to collagenous extracellular matrix, rather than GAG molecules themselves.

Finally, regarding CA4+ incubation time, both the 24 and 30 hours incubations provided strong x-ray attenuation for unfixed and NBF-fixed cartilage when compared to the 8 hours incubation. Although the 24 hours incubation yielded slightly lower x-ray attenuation compared to the 30 hours, in both unfixed and NBF-fixed groups, the cartilage was easily distinguishable from the subchondral bone. Furthermore, the 24 hours incubation time was convenient for performing *ex vivo* experiments. However, given that the 8 hours incubation time also achieved effective contrast between cartilage signaling and subchondral bone, this time of incubation may be suitable for *in vivo* studies such as intraarticular injection for live imaging. Additionally, since PBS soaking significantly decreased the signal in unfixed cartilage after imaging, it is likely CA4+ will diffuse out from cartilage over time into the physiological environment of joint fluid which has similar pH as PBS. Therefore, this technique may be suitable for *in vivo* cartilage imaging. This is corroborated by a recent study investigating equine clinical CA4+ CECT, which showed that CECT can be captured 4 hours after CA4+ injection [38].

Conclusion

In summary, CA4+ CECT of both unfixed and NBF fixed cartilage tissues enables accurate and facile cartilage quantification and morphological assessment. Importantly, it is feasible to perform downstream H&E, Alcian blue, Safranin O, and Col2 immunohistochemical staining after decalcification with EDTA for unfixed tissue labeled with CA4+. This regimen allows investigators to obtain both quantitative microCT data and histology data on the same tissue specimen allowing for lower cost and processing time, while being labor efficient. Furthermore, because the CA4+ binding to unfixed cartilage is reversible and can be washed out by PBS, it is suitable for *in vivo* CECT imaging cartilage. NBF fixed cartilage tissues, labeled with CA4+, are more distinguishable (intense) from subchondral bone by microCT than unfixed cartilage and can be subsequently stained with H&E and Alcian blue after decalcification with EDTA. However, it is not feasible to perform Safranin O staining and immunohistochemistry after CA4+ labelling of NBF fixed tissues. CA4+ is a promising contrast enhancement reagent for cartilage imaging and quantification *ex vivo* and *in vivo*.

Acknowledgements

This project was funded by NIH R21 grant (R21AR066206-03) and the Steven and Mary Read Foundation. We thank Sarah Amra for processing and embedding parts of the tissues for histology and Gilberto Nakama and Haizi Cheng for help of harvesting rabbit femurs. We thank Dylan Rakowski from The Center for Outcomes-Based Orthopaedic Research, Steadman Philippon Research Institute for proofreading the manuscript during revision.

Disclosure of conflict of interest

JH received Royalties from Cooke Myocytes annually. Dr. Philippon, Education payments from Linvatec (2015); speaking fees and consulting fees from Smith & Nephew (through 2018), Synthes GmbH (2019); royalties from DJO (2015/16), Linvatec (through 2018), and Smith & Nephew (2015/16); and hospitality payments from Siemens Medical Solutions (2016).

Address correspondence to: Dr. Johnny Huard, Chief Scientific Officer and Director of the Center for Regenerative Sports Medicine, Steadman Philippon Research Institute, 181 W Meadow Dr, Suite 1000, Vail, CO 81657, USA. E-mail: jhuard@sprivail.org

References

[1] Chinzei N, Rai MF, Hashimoto S, Schmidt EJ, Takebe K, Cheverud JM and Sandell LJ. Evidence for genetic contribution to variation in posttraumatic osteoarthritis in mice. Arthritis Rheumatol 2019; 71: 370-381.

[2] Rai MF, Hashimoto S, Johnson EE, Janiszak KL, Fitzgerald J, Heber-Katz E, Cheverud JM and Sandell LJ. Heritability of articular cartilage regeneration and its association with ear wound healing in mice. Arthritis Rheum 2012; 64: 2300-2310.

[3] Deng Z, Gao X, Sun X, Amra S, Lu A, Cui Y, Eltzschig HK, Lei G and Huard J. Characterization of articular cartilage homeostasis and the mechanism of superior cartilage regeneration of MRL/MpJ mice. FASEB J 2019; 33: 8809-8821.

[4] Xie J, Zhang D, Lin Y, Yuan Q and Zhou X. Anterior cruciate ligament transection-induced cellular and extracellular events in menisci: implications for osteoarthritis. Am J Sports Med 2018; 46: 1185-1198.

[5] Saito M, Sasho T, Yamaguchi S, Ikegawa N, Akagi R, Muramatsu Y, Mukoyama S, Ochiai N, Nakamura J, Nakagawa K, Nakajima A and Takahashi K. Angiogenic activity of subchondral bone during the progression of osteoarthritis in a rabbit anterior cruciate ligament transection model. Osteoarthritis Cartilage 2012; 20: 1574-1582.

[6] van den Bosch MH, Blom AB, Kram V, Maeda A, Sikka S, Gabet Y, Kilts TM, van den Berg WB, van Lent PL, van der Kraan PM and Young MF. WISP1/CCN4 aggravates cartilage degeneration in experimental osteoarthritis. Osteoarthritis Cartilage 2017; 25: 1900-1911.

[7] Sampson ER, Beck CA, Ketz J, Canary KL, Hilton MJ, Awad H, Schwarz EM, Chen D, O'Keefe RJ, Rosier RN and Zuscik MJ. Establishment of an index with increased sensitivity for assessing murine arthritis. J Orthop Res 2011; 29: 1145-1151.

[8] Wang M, Sampson ER, Jin H, Li J, Ke QH, Im HJ and Chen D. MMP13 is a critical target gene during the progression of osteoarthritis. Arthritis Res Ther 2013; 15: R5.

[9] Zhang Y, Sheu TJ, Hoak D, Shen J, Hilton MJ, Zuscik MJ, Jonason JH and O'Keefe RJ. CCN1 regulates chondrocyte maturation and cartilage development. J Bone Miner Res 2016; 31: 549-559.

[10] Hamada D, Sampson ER, Maynard RD and Zuscik MJ. Surgical induction of posttraumatic osteoarthritis in the mouse. Methods Mol Biol 2014; 1130: 61-72.

[11] Gao X, Cheng H, Awada H, Tang Y, Amra S, Lu A, Sun X, Lv G, Huard C, Wang B, Bi X, Wang Y and Huard J. A comparison of BMP2 delivery by coacervate and gene therapy for promoting human muscle-derived stem cell-mediated articular cartilage repair. Stem Cell Res Ther 2019; 10: 346.

[12] Rai MF, Brophy RH and Sandell LJ. Osteoarthritis following meniscus and ligament injury: insights from translational studies and animal models. Curr Opin Rheumatol 2019; 31: 70-79.

[13] Blaker CL, Clarke EC and Little CB. Using mouse models to investigate the pathophysiology, treatment, and prevention of post-traumatic osteoarthritis. J Orthop Res 2017; 35: 424-439.

[14] Christiansen BA, Guilak F, Lockwood KA, Olson SA, Pitsillides AA, Sandell LJ, Silva MJ, van der Meulen MC and Haudenschild DR. Non-invasive mouse models of post-traumatic osteoarthritis. Osteoarthritis Cartilage 2015; 23: 1627-1638.

[15] Deng Z, Gao X, Sun X, Amra S, Lu A, Cui Y, Eltzschig HK, Lei G and Huard J. Characterization of articular cartilage homeostasis and the mechanism of superior cartilage regeneration of MRL/MpJ mice. FASEB J 2019; 33: 8809-8821.

[16] Matsumoto T, Cooper GM, Gharaibeh B, Meszaros LB, Li G, Usas A, Fu FH and Huard J. Cartilage repair in a rat model of osteoarthritis through intraarticular transplantation of muscle-derived stem cells expressing bone morphogenetic protein 4 and soluble Flt-1. Arthritis Rheum 2009; 60: 1390-1405.

[17] Bouxsein ML, Boyd SK, Christiansen BA, Guldberg RE, Jepsen KJ and Muller R. Guidelines for assessment of bone microstructure in rodents using micro-computed tomography. J Bone Miner Res 2010; 25: 1468-1486.

[18] Das Neves Borges P, Forte AE, Vincent TL, Dini D and Marenzana M. Rapid, automated imaging of mouse articular cartilage by microCT for early detection of osteoarthritis and finite element modelling of joint mechanics. Osteoarthritis Cartilage 2014; 22: 1419-1428.

[19] Nieminen HJ, Gahunia HK, Pritzker KPH, Ylitalo T, Rieppo L, Karhula SS, Lehenkari P, Haeggstrom E and Saarakkala S. 3D histopathological grading of osteochondral tissue using contrast-enhanced micro-computed tomography. Osteoarthritis Cartilage 2017; 25: 1680-1689.

[20] Kerckhofs G, Sainz J, Wevers M, Van de Putte T and Schrooten J. Contrast-enhanced nanofocus computed tomography images the cartilage subtissue architecture in three dimensions. Eur Cell Mater 2013; 25: 179-189.

[21] Thote T, Lin AS, Raji Y, Moran S, Stevens HY, Hart M, Kamath RV, Guldberg RE and Willett

NJ. Localized 3D analysis of cartilage composition and morphology in small animal models of joint degeneration. Osteoarthritis Cartilage 2013; 21: 1132-1141.

[22] Joshi NS, Bansal PN, Stewart RC, Snyder BD and Grinstaff MW. Effect of contrast agent charge on visualization of articular cartilage using computed tomography: exploiting electrostatic interactions for improved sensitivity. J Am Chem Soc 2009; 131: 13234-13235.

[23] Stewart RC, Patwa AN, Lusic H, Freedman JD, Wathier M, Snyder BD, Guermazi A and Grinstaff MW. Synthesis and preclinical characterization of a cationic iodinated imaging contrast agent (CA4+) and its use for quantitative computed tomography of ex vivo human hip cartilage. J Med Chem 2017; 60: 5543-5555.

[24] Lakin BA, Grasso DJ, Stewart RC, Freedman JD, Snyder BD and Grinstaff MW. Contrast enhanced CT attenuation correlates with the GAG content of bovine meniscus. J Orthop Res 2013; 31: 1765-1771.

[25] Oh DJ, Lakin BA, Stewart RC, Wiewiorski M, Freedman JD, Grinstaff MW and Snyder BD. Contrast-enhanced CT imaging as a non-destructive tool for ex vivo examination of the biochemical content and structure of the human meniscus. J Orthop Res 2017; 35: 1018-1028.

[26] Stewart RC, Nelson BB, Kawcak CE, Freedman JD, Snyder BD, Goodrich LR and Grinstaff MW. A contrast-enhanced computed tomography scoring system for distinguishing early osteoarthritis disease states: a feasibility study. J Orthop Res 2019; 37: 2138-2148.

[27] Nelson BB, Mäkelä JTA, Lawson TB, Patwa AN, Snyder BD, McIlwraith CW, Grinstaff MW, Goodrich LR and Kawcak CE. Cationic contrast-enhanced computed tomography distinguishes between reparative, degenerative, and healthy equine articular cartilage. J Orthop Res 2020; [Epub ahead of print].

[28] Bhattarai A, Honkanen JTJ, Myller KAH, Prakash M, Korhonen M, Saukko AEA, Virén T, Joukainen A, Patwa AN, Kröger H, Grinstaff MW, Jurvelin JS and Töyräs J. Quantitative dual contrast CT technique for evaluation of articular cartilage properties. Ann Biomed Eng 2018; 46: 1038-1046.

[29] Freedman JD, Ellis DJ, Lusic H, Varma G, Grant AK, Lakin BA, Snyder BD and Grinstaff MW. dGEMRIC and CECT comparison of cationic and anionic contrast agents in cadaveric human metacarpal cartilage. J Orthop Res 2020; 38: 719-725.

[30] Hayward LN, de Bakker CM, Gerstenfeld LC, Grinstaff MW and Morgan EF. Assessment of contrast-enhanced computed tomography for imaging of cartilage during fracture healing. J Orthop Res 2013; 31: 567-573.

[31] Stewart RC, Bansal PN, Entezari V, Lusic H, Nazarian RM, Snyder BD and Grinstaff MW. Contrast-enhanced CT with a high-affinity cationic contrast agent for imaging ex vivo bovine, intact ex vivo rabbit, and in vivo rabbit cartilage. Radiology 2013; 266: 141-150.

[32] Garcia JP, Longoni A, Gawlitta D, A JWPR, Grinstaff MW, Toyras J, Weinans H, Creemers LB and Pouran B. Contrast enhanced computed tomography for real-time quantification of glycosaminoglycans in cartilage tissue engineered constructs. Acta Biomater 2019; 100: 202-212.

[33] Nickmanesh R, Stewart RC, Snyder BD, Grinstaff MW, Masri BA and Wilson DR. Contrast-enhanced computed tomography (CECT) attenuation is associated with stiffness of intact knee cartilage. J Orthop Res 2018; 36: 2641-2647.

[34] Lakin BA, Patel H, Holland C, Freedman JD, Shelofsky JS, Snyder BD, Stok KS and Grinstaff MW. Contrast-enhanced CT using a cationic contrast agent enables non-destructive assessment of the biochemical and biomechanical properties of mouse tibial plateau cartilage. J Orthop Res 2016; 34: 1130-1138.

[35] Mashiatulla M, Moran MM, Chan D, Li J, Freedman JD, Snyder BD, Grinstaff MW, Plaas A and Sumner DR. Murine articular cartilage morphology and compositional quantification with high resolution cationic contrast-enhanced muCT. J Orthop Res 2017; 35: 2740-2748.

[36] Dourthe B, Nickmanesh R, Wilson DR, D'Agostino P, Patwa AN, Grinstaff MW, Snyder BD and Vereecke E. Assessment of healthy trapeziometacarpal cartilage properties using indentation testing and contrast-enhanced computed tomography. Clin Biomech (Bristol, Avon) 2019; 61: 181-189.

[37] Honkanen MKM, Matikka H, Honkanen JTJ, Bhattarai A, Grinstaff MW, Joukainen A, Kroger H, Jurvelin JS and Toyras J. Imaging of proteoglycan and water contents in human articular cartilage with full-body CT using dual contrast technique. J Orthop Res 2019; 37: 1059-1070.

[38] Nelson BB, Makela JTA, Lawson TB, Patwa AN, Barrett MF, McIlwraith CW, Hurtig MB, Snyder BD, Moorman VJ, Grinstaff MW, Goodrich LR and Kawcak CE. Evaluation of equine articular cartilage degeneration after mechanical impact injury using cationic contrast-enhanced computed tomography. Osteoarthritis Cartilage 2019; 27: 1219-1228.

[39] Utsunomiya H, Gao X, Deng Z, Cheng H, Nakama G, Scibetta AC, Ravuri SK, Goldman JL, Lowe WR, Rodkey WG, Alliston T, Philippon MJ and Huard J. Biologically regulated marrow stimulation by blocking TGF-beta1 with losartan oral administration results in hyaline-like

cartilage repair: a rabbit osteochondral defect model. Am J Sports Med 2020; 48: 974-984.
[40] Utsunomiya H, Gao X, Cheng H, Deng Z, Nakama G, Mascarenhas R, Goldman JL, Ravuri SK, Arner JW, Ruzbarsky JJ, Lowe WR, Philippon MJ and Huard J. Intra-articular injection of bevacizumab enhances bone marrow stimulation-mediated cartilage repair in a rabbit osteochondral defect model. Am J Sports Med 2021; 49: 1871-1882.
[41] Bhattarai A, Pouran B, Mäkelä JTA, Shaikh R, Honkanen MKM, Prakash M, Kröger H, Grinstaff MW, Weinans H, Jurvelin JS and Töyräs J. Dual contrast in computed tomography allows earlier characterization of articular cartilage over single contrast. J Orthop Res 2020; 38: 2230-2238.
[42] Bansal PN, Stewart RC, Entezari V, Snyder BD and Grinstaff MW. Contrast agent electrostatic attraction rather than repulsion to glycosaminoglycans affords a greater contrast uptake ratio and improved quantitative CT imaging in cartilage. Osteoarthritis Cartilage 2011; 19: 970-976.
[43] Lakin BA, Ellis DJ, Shelofsky JS, Freedman JD, Grinstaff MW and Snyder BD. Contrast-enhanced CT facilitates rapid, non-destructive assessment of cartilage and bone properties of the human metacarpal. Osteoarthritis Cartilage 2015; 23: 2158-2166.
[44] Bagi CM, Berryman E, Zakur DE, Wilkie D and Andresen CJ. Effect of antiresorptive and anabolic bone therapy on development of osteoarthritis in a posttraumatic rat model of OA. Arthritis Res Ther 2015; 17: 315.
[45] Fu M, Liu J, Huang G, Huang Z, Zhang Z, Wu P, Wang B, Yang Z and Liao W. Impaired ossification coupled with accelerated cartilage degeneration in developmental dysplasia of the hip: evidences from muCT arthrography in a rat model. BMC Musculoskelet Disord 2014; 15: 339.
[46] Benders KE, Malda J, Saris DB, Dhert WJ, Steck R, Hutmacher DW and Klein TJ. Formalin fixation affects equilibrium partitioning of an ionic contrast agent-microcomputed tomography (EPIC-muCT) imaging of osteochondral samples. Osteoarthritis Cartilage 2010; 18: 1586-1591.
[47] Reece DS, Thote T, Lin ASP, Willett NJ and Guldberg RE. Contrast enhanced muCT imaging of early articular changes in a pre-clinical model of osteoarthritis. Osteoarthritis Cartilage 2018; 26: 118-127.
[48] Willett NJ, Thote T, Hart M, Moran S, Guldberg RE and Kamath RV. Quantitative pre-clinical screening of therapeutics for joint diseases using contrast enhanced micro-computed tomography. Osteoarthritis Cartilage 2016; 24: 1604-1612.
[49] Maerz T, Newton MD, Kristof K, Motovylyak O, Fischgrund JS, Park DK and Baker KC. Three-dimensional characterization of in vivo intervertebral disc degeneration using EPIC-muCT. Osteoarthritis Cartilage 2014; 22: 1918-1925.

Supplementary Video 1. Continuous view of CA+ CECT images of 24-hour labeling of NBF fixed cartilage immediately after labeling. Both trochlear groove and condyle cartilage are clearly imaged and show higher density than subchondral bone. Cartilage is clearly distinct from subchondral bone.

Supplementary Video 2. Continuous view of CA4+ CECT images of 24-hour labeling of unfixed cartilage right after labeling. Both trochlear groove and condyle cartilage are visible and show higher density than subchondral bone.

Supplementary Video 3. Continuous view of CA4+ CECT images for 24-hour labeling of unfixed cartilage after decalcification. Cartilage regions are not visible. Subchondral bone is also not visible due to decalcification. High background is due to no signal.

Supplementary Video 4. Continuous view of CA4+ CECT images for 24-hour labeling of NBF fixed cartilage after decalcification. Cartilage regions are clearly distinguishable while subchondral bone is invisible due to decalcification. Subchondral trabecular bone in certain area is still visible due to incomplete decalcification.